HHS Public Access

Author manuscript

Sci Immunol. Author manuscript; available in PMC 2016 December 05.

Published in final edited form as:

Sci Immunol. 2016 October ; 1(4): .

Type I interferon suppresses virus-specific B cell responses by modulating CD8+ T cell differentiation

E. Ashley Moseman[1], **Tuoqi Wu**[2], **Juan Carlos de la Torre**[3], **Pamela L. Schwartzberg**[2], and **Dorian B. McGavern**[1,*]

[1]Viral Immunology and Intravital Imaging Section, National Institute of Neurological Disorders and Stroke, National Institutes of Health, Bethesda, MD 20892, USA

[2]National Human Genome Research Institute, National Institutes of Health, Bethesda, MD 20892, USA

[3]Scripps Research Institute, La Jolla, CA 92037, USA

Abstract

Studies have established a role for T cells in resolving persistent viral infections, yet emerging evidence indicates that both T and B cells are required to control some viruses. During persistent infection, a marked lag or failure to generate neutralizing antibodies is commonly observed and likely contributes to an inability to control certain pathogens. Using lymphocytic choriomeningitis virus (LCMV) as a model, we have examined how a persistent viral infection can suppress neutralizing humoral immunity. By tracking the fate of virus-specific B cells in vivo, we report that LCMV-specific B cells were rapidly deleted within a few days of persistent infection, and this deletion was completely reversed by blockade of type I interferon (IFN-I) signaling. Early interference with IFN-I signaling promoted survival and differentiation of LCMV-specific B cells, which accelerated the generation of neutralizing antibodies. This marked improvement in antiviral humoral immunity did not rely on the cessation of IFN-I signaling in B cells but on alterations in the virus-specific $CD8^+$ T cell response. Using two-photon microscopy and in vivo calcium imaging, we observed that cytotoxic T lymphocytes (CTLs) productively engaged and killed

*Corresponding author. mcgavernd@mail.nih.gov.

SUPPLEMENTARY MATERIALS

immunology.sciencemag.org/cgi/content/full/1/4/eaah3565/DC1

Materials and Methods

Fig. S1. Effects of IFNAR blockade and virus strain or titer on LCMV-specific B cells.

Fig. S2. CTL engagement of antiviral B cells and control LCMV-iCre–infected Confetti mice.

Movie S1. LCMV-specific B cells thrive upon late transfer into infected hosts.

Movie S2. IFNAR blockade prevents deletion of LCMV-specific B cells.

Movie S3. LCMV-specific CTLs flux calcium upon contact with LCMV-specific B cells.

Movie S4. Antiviral CTLs productively engage LCMV-specific B cells.

Movie S5. LCMV-specific B cells are killed in vivo.

Movie S6. LCMV-infected B cells contribute to clonal GCs in the absence of functional CTLs.

Table S1. Excel file containing tabulated data for Figs. 1 to 7 and fig. S1.

References (*66*–*72*)

Author contributions: E.A.M. and D.B.M. designed the experiments. E.A.M. completed all experiments. E.A.M. and D.B.M. wrote the manuscript. D.B.M. provided the funding. T.W. and P.L.S. generated the GCaMP6s reporter mice. J.C.T. generated LCMV-iCre. E.A.M. and D.B.M. analyzed data and carried out the statistical analyses.

Competing interests: The authors declare that they have no competing interests.

LCMV-specific B cells in a perforin-dependent manner within the first few days of infection. Blockade of IFN-I signaling protected LCMV-specific B cells by promoting CTL dysfunction. Therapeutic manipulation of this pathway may facilitate efforts to promote humoral immunity during persistent viral infection in humans. Our findings illustrate how events that occur early after infection can disturb the resultant adaptive response and contribute to viral persistence.

INTRODUCTION

Humoral responses depend in part on B cells engaging cognate antigens and interacting with $CD4^+$ helper T cells. This is usually followed by the subsequent coordination of antibody-secreting cell (ASC) differentiation, germinal center (GC) development to facilitate antibody affinity maturation, and memory B cell generation (1, 2). Because humoral responses are simultaneously susceptible to shifts in direct costimulatory and inhibitory signals to B cells, as well as those that affect the differentiation and activation of their partner $CD4^+$ helper T cells, driving a successful anti-pathogen humoral immune response is highly dependent upon the pathogen in question (1, 3). In particular, viral infections exhibit different patterns, with some being cleared rapidly and others establishing long-term persistence (4, 5). In animals, disruptions in humoral immunity due to disturbances in the B cell compartment or $CD4^+$ helper T cell functions compromise antiviral immunity to numerous viral pathogens (6–9). Chronic noncytopathic viral infections, such as hepatitis C virus (HCV), hepatitis B virus (HBV), HIV, and lymphocytic choriomeningitis virus (LCMV), elicit poor neutralizing antibody responses even after the acute phase of viral replication has passed (10–13). In mice, intravenous inoculation with the Armstrong strain of LCMV results in an acute infection that is typically cleared within 1 week (14). By contrast, infection with persistence-prone strains, such as clone 13 (CL13), results in prolonged viremia and viral reservoir occupancy, similar to that observed in chronic human infections (5, 14–16). Study of the LCMV model has generated numerous insights into T and B cell biology (13, 17, 18).

Chronic viral infections are known to perturb B cell responses, typically resulting in excessive proliferation and differentiation, as well as ectopic follicle formation (19–21). The development of neutralizing antibodies to CL13 is substantially delayed, and serum viral titers often decline to undetectable levels before neutralizing antibodies to the virus emerge (22). Consequently, B cells and humoral immunity, in general, were postulated to play no role in viral clearance, even though LCMV infection elicits a very large humoral response that is almost entirely directed toward nonneutralizing epitopes (13). Although nonneutralizing specificities have been shown to be beneficial (22, 23), the failure to generate neutralizing antibodies to LCMV has been a source of much investigation over the past several decades.

Many factors were shown to negatively affect neutralizing antibody development after LCMV infection. Several of these factors stem from the magnitude of the $CD8^+$ and $CD4^+$ T cell responses elicited by LCMV (24, 25). Specifically, earlier studies reported that cytotoxic T lymphocyte (CTL)–mediated disruptions in normal splenic architecture and chemokine guidance create antigen nonspecific immunosuppression (26, 27). Similarly, the massive $CD4^+$ T cell expansion and T follicular helper lineage commitment bias after infection was

also shown to impair humoral immunity because partial removal of $CD4^+$ T helper cell function resulted in accelerated neutralizing antibody responses (28).

Another hypothesis set forth to explain the delayed development of LCMV-specific neutralizing antibodies is that the endogenous B cell repertoire lacks reactivity against the LCMV glycoprotein (GP) or that B cells with this reactivity simply fail to expand after infection (29). A sophisticated series of GP-swapping experiments between vesicular stomatitis virus (VSV) and LCMV revealed that the LCMV-GP elicited a poor neutralizing antibody response regardless of virion backbone, suggesting a low B cell precursor frequency (29). By contrast, a contentious study reported that LCMV-neutralizing B cells are relatively numerous in the naïve repertoire but are deleted by $CD8^+$ T cells after infection (30). Antibodies against the LCMV-GP are produced after infection, albeit with delayed kinetics and at lower levels relative to anti-nucleoprotein antibodies (31). Although it is difficult to reconcile these studies, it is conceivable that multiple mechanisms contribute to suboptimal neutralizing antibody responses during states of persistent viral infection.

We sought to gain insights into the early events that shape the fate of LCMV-GP–specific B cells at the outset of persistent viral infection and to develop a therapeutic approach to rescuing these cells and fostering accelerated production of neutralizing antibodies. Through imaging and multicolor lineage tracing studies, we monitored the in vivo dynamics of LCMV-GP–specific B cells at early time points after infection and followed their fate over time. Using a calcium reporter mouse to monitor cell-cell interactions, we revealed that CTLs productively engage and use perforin to kill LCMV-specific B cells that express a neutralizing B cell receptor (BCR) within a few days of infection. Blockade of type I interferon (IFN-I) signaling prevented deletion of LCMV-specific B cells and promoted an accelerated development of neutralizing antibodies. We found that early blockade of IFN-I promotes CTL dysfunction, allowing infected LCMV-specific B cells to survive and contribute to GC reactions. Using B cell fate mapping, we have confirmed that clonal populations of LCMV-infected B cells only survive when IFN-I signaling is blocked and CTLs are rendered dysfunctional.

RESULTS

IFN-I receptor blockade preserves virus-specific B cells

To explore the neutralizing B cell response to chronic LCMV infection, we used a BCR heavy-chain knock-in transgenic (tg) mouse specific for LCMV-WE GP (KL25) (32). In these mice, ~10% of mature B cells express a light chain pairing that forms a neutralizing BCR against a reverse genetically modified mutant of LCMV CL13, dubbed LCMV-M1 (33). Previous reports have shown that KL25 transfer into mice before infection can lead to early production of neutralizing antibodies; however, these cells rapidly disappear (34). To monitor the fate of LCMV-GP–specific B cells in vivo, we adoptively transferred naïve $mCerulean^+$ $Blimp1\text{-}YFP^+$ KL25 cells into C57BL/6J (B6) hosts and then infected them with a persistent dose of LCMV-M1. KL25 cells transferred into mice before infection were deleted after challenge with LCMV-M1 (Fig. 1, A and B). However, when KL25 cells were adoptively transferred into mice 6 days after infection, they not only survived (Fig. 1, A and B) but also differentiated into $Blimp1\text{-}YFP^+$ ASCs (Fig. 1A). When analyzed at 2 to 3 weeks

after transfer, KL25 cells transferred 6 days after infection were found proliferating ($Ki67^+$) within splenic GCs (Fig. 1D). By contrast, very few KL25 cells were present in the spleens of the mice receiving KL25 cells before infection (Fig. 1C). Examination of splenic B cell dynamics by in vivo two-photon microscopy (TPM) revealed classic GC interactions between KL25 B cells transferred 6 days after infection and LCMV-specific $CD4^+$ T cells (movie S1).

LCMV infection, like other chronic viral infections including HCV and HBV, is associated with prolonged IFN-I production (35–37). Recently, it has been shown that early blockade of IFN-I signaling can result in enhanced immune functionality and accelerated clearance of LCMV CL13 (35, 38, 39). Because the surge in IFN-I production largely subsides by day 6 after infection (35), we hypothesized that early high-level IFN-I receptor (IFNAR) signaling was responsible for KL25 deletion. We administered blocking antibodies against IFNAR (αIFNAR) concurrently with $mCerulean^+Blimp1\text{-}YFP^+$KL25 cells 1 day before infection with LCMV-M1 (Fig. 1,A, B, and E). IFNAR blockade completely reversed the deletion of KL25 cells, resulting in numbers comparable to those observed when KL25 cells were transferred after infection. These flow cytometry data were further supported by in vivo TPM (movie S2) and immunohistochemical studies (Fig. 1, F and G) on the spleen 7 days after infection, which revealed a massive accumulation of $mCerulean^+Blimp1\text{-}YFP^+$KL25 cells in mice treated with αIFNAR compared with those treated with isotype control antibodies, with ~95% of these being CD138-expressing ASCs (Fig. 1, H and I). The effects of αIFNAR were long term because treatment increased splenic cellularity, including $GL7^+$ KL25 B cells and $CD138^+$ ASCs, at 30 days after infection (fig. S1, A to D).

KL25 cells can bind but not neutralize another reverse genetically modified mutant of LCMV CL13, dubbed LCMV-M2 (33). Upon LCMV-M2 infection, KL25 cells are deleted similarly to LCMV-M1 infection, and this deletion is rescued by αIFNAR (fig. S1E).We also found that KL25 cells are deleted in mice infected with a lower dose [4×10^4 plaque-forming units (PFU)] of LCMV-M1, which is cleared acutely (fig. S1E).

Inhibition of IFN-I signaling accelerates endogenous neutralizing antibody production

Given that IFNAR blockade markedly improved KL25 survival, expansion, and differentiation after LCMV-M1 infection, we next evaluated whether the same benefit would apply to endogenous LCMV-specific B cells by assessing the development of serum LCMV-neutralizing antibodies in mice treated with αIFNAR or isotype control antibodies, infected with LCMV-M1, and monitored over time. IFNAR blockade consistently accelerated the generation of neutralizing antibodies against LCMV-M1 (Fig. 2A). These findings were confirmed after infection with wild-type (WT) CL13 (Fig. 2B), indicating that the response to LCMV-M1 is not unique.

To examine the early effects of IFNAR blockade on the endogenous B cell repertoire, we generated hybridomas from the spleens of isotype control–treated versus αIFNAR-treated mice at day 7 after infection (Fig. 2C). At this time point, spleens from αIFNAR-treated mice were several-fold larger than those from isotype control–treated mice, contained a higher percentage of $CD138^+$ cells (Fig. 1, H and I), and thus yielded a high number of hybridoma clones relative to the isotype control group (>360 versus 60, respectively). None

of the antibodies obtained from the 420 hybridomas analyzed neutralized LCMV; however, a higher percentage of hybridomas obtained from αIFNAR-treated mice produced antibodies that bound to plates coated with purified LCMV or a GP-Fc fusion protein (Fig. 2C). Considering the vastly greater number of hybridomas generated per mouse, we estimate that at least 10-fold more LCMV-GP–specific B cells were present in each αIFNAR-treated mouse on day 7 compared with isotype control–treated mice (43 versus 4 reactive clones).

IFN-I induces deletion of LCMV-specific B cells in a cell-extrinsic manner

The strong prosurvival benefit of IFNAR blockade on KL25 cells after LCMV-M1 infection led us to examine whether LCMV infection induced a broadly hostile environment for B cells within the infected spleen. We took advantage of another BCR-tg mouse (referred to as VI10YEN) containing a heavy-chain knock-in and light-chain transgene specific for the GP of VSV Indiana (32) to serve as bystander B cells in our studies. Adoptive cotransfer of KL25 and VI10YEN cells into mice revealed that both cell types survive equally well in naïve animals (Fig. 3, A and B). However, after infection with LCMV-M1,KL25 cells were specifically deleted, whereas the number of VI10YEN cells was unchanged even after IFNAR blockade (Fig. 3, A and B), indicating that high-level IFNAR signaling shortly after LCMV infection did not ablate mature B cells in general but rather deleted LCMV-specific B cells.

Previous work on IFNAR signaling in antiviral B cells has indicated that IFNAR augments B cell expansion after VSV infection (40); however, we postulated that if IFNAR signaling combined with BCR ligation to reduce KL25 viability, then deletion of IFNAR from KL25 cells would enhance their survival after infection. We used two approaches to examine the intrinsic role of IFNAR in KL25 B cells. First, we adoptively transferred WT KL25 cells into IFNAR$^{-/-}$ mice and compared their survival with that in B6 mice treated with αIFNAR antibodies (Fig. 3C). KL25 cells survived and expanded comparably in these two environments, suggesting that IFNAR blockade promoted LCMV-specific B cell survival in a cell-extrinsic manner. To further test this hypothesis, we transferred CD45.1^{+}IFNAR$^{-/-}$ KL25 B cells and compared them with WT KL25 cells transferred into the same B6 host. WT and IFNAR$^{-/-}$ KL25 cells survived comparably when transferred into naïve B6 mice (Fig. 3, D to F). However, after infection with LCMV-M1, IFNAR$^{-/-}$ KL25 cells showed no survival advantage relative to WT cells (Fig. 3, D to F). Both WT and IFNAR$^{-/-}$ KL25 cells survived better in αIFNAR-treated mice than in isotype control–treated animals (Fig. 3F), but WT cells had a distinct survival advantage—they outnumbered IFNAR$^{-/-}$ cells (in a ratio of 10:1) (Fig. 3, E and G). These data indicate that at least some residual IFNAR signaling was present at this time point despite the αIFNAR treatment and that IFN-I was not inherently detrimental to B cells. These data also support the conclusion that IFNAR blockade rescues KL25 cells in a cell-extrinsic manner.

CD8 T cell depletion rescues LCMV-specific B cells similarly to IFNAR blockade

Because the effect of IFNAR blockade on LCMV-GP B cells was cell-extrinsic, we set out to identify the IFNAR-dependent cell population(s) responsible for KL25 deletion. Hematopoietic cells other than dendritic cells can present viral antigens to B cells in vivo (41). After intravenous LCMV inoculation, marginal zone macrophages are virally infected

(42, 43), making them a reliable source of continued high-level antigen production and presentation to B cells. To test whether proximity to phagocytes in this region might facilitate their engulfment and deletion, we intravenously injected mice with clodronate liposomes to deplete monocytes and marginal zone macrophages (42). Clodronate pretreatment did not increase KL25 survival 7 days after LCMV-M1 infection, nor did depletion of neutrophils and monocytes through administration of αLy6G and αLy6c antibodies, respectively (Fig. 4A). $CD4^+$ T cells are required for continued anti-LCMV immunoglobulin G (IgG) production after persistent infection (44); however, depletion of CD4 T cells or natural killer (NK) cells did not affect KL25 survival (Fig. 4B). In contrast, $CD8^+$ T cell depletion resulted in preservation of KL25 cells to a level approaching that observed in αIFNAR-treated animals (Fig. 4C). KL25 cells survived comparably in ovalbumin T cell receptor (TCR) transgenic mice (OT-I) (45) hosts whose $CD8^+$ T cell repertoire was constrained to ovalbumin reactivity (Fig. 4C), ruling out effects of the CD8α-depleting antibody on other CD8α-expressing cell types. Reversal of early B cell death by CD8 depletion was evident by day 3 after infection (Fig. 4D). We could also detect LCMV protein in KL25 B cells at 24 hours after infection (Fig. 4E), and 8800 infectious centers per 1×10^6 sorted KL25 B cells remained detectable at 3 days after infection, supporting the direct infection of KL25 B cells by LCMV. KL25 B cells from αIFNAR mice showed evidence of greater proliferation (Fig. 4F) and activation (such as IgM down-regulation) (Fig. 4G) compared with CD8-depleted and isotype control–treated animals, indicating an additional benefit of IFNAR blockade on humoral immunity.

IFNAR signaling is required for early CTL differentiation and LCMV-specific B cell deletion

Inflammatory cytokines, such as IFN-I and interleukin-12 (IL-12), are known to drive effector $CD8^+$ T cell differentiation (46). On the basis of our KL25 survival studies, we postulated that impeding IFN-I signaling through IFNAR blockade might also alter virus-specific $CD8^+$ T cell differentiation and acquisition of effector functions at early time points after infection, which would in turn negate CTL-mediated killing of KL25 cells. To evaluate the impact of IFNAR blockade on CTL differentiation, we adoptively transferred $Thy1.1^+CD8^+$TCR-tg T cells specific for the LCMV-GP (P14 cells) (47) into mice treated with either isotype or αIFNAR antibodies and then infected with LCMV-M1. Between days 3 and 4 after infection, we observed that P14 T cells from αIFNAR-treated mice produced less IFN-γ than did isotype controls to endogenously presented viral antigen (Fig. 5, A and C). After addition of cognate peptide ($GP_{33–41}$), P14 cells from αIFNAR mice produced less IFN-γ (Fig. 5, A and D) and tumor necrosis factor–α (TNFα) (Fig. 5, B and E) than did isotype control cells.

In addition to cytokine production, we also examined the cytolytic functions of IFNAR-blocked CTLs. Granzyme B was markedly reduced in P14 cells obtained from αIFNAR-treated mice 3 days after LCMV-M1 infection (Fig. 5, F and G), further supporting an early negative impact on CTL functionality. To gauge the impact of IFNAR blockade on CTL lytic function, we cocultured splenic P14 cells isolated at day 3.5 after infection with cognate peptide-pulsed targets. Control P14 cells killed steadily over the 5-hour incubation period, whereas CTLs from αIFNAR mice showed only a slight increase in killing above the 0-hour time point (Fig. 5H).

Impairment of CD8$^+$ T cell cytolytic function results in preservation of LCMV-specific B cells after infection

The reduced granzyme B expression and impaired cytolytic function of effector CD8$^+$ T cells from IFNAR-blocked animals (Fig. 5, F to H), combined with detectable infection of KL25 B cells (Fig. 4E), led us to test whether perforin (PRF1)–dependent CD8$^+$ T cell cytolytic function was directly responsible for KL25 deletion after LCMV-M1 infection. Seven days after infection, KL25 survival in PRF1$^{-/-}$ mice was equivalent to survival in CD8-depleted mice (Fig. 6A) and included more CD138$^+$ ASC differentiation (Fig. 6B), indicating that cytolytic function is responsible for the collapse in KL25 numbers. To analyze LCMV-specific B cells at early time points after infection, we used KL25 heavy- and light-chain double-transgenic mice (KL25 H+L) to ensure that the observed cells and interactions involved a neutralizing B cell specificity. Immunohistochemical analyses of αIFNAR-, αCD8-, and isotype control antibody–treated mice, as well as PRF1$^{-/-}$ mice, at day 3 after infection revealed that KL25 H+L B cells were mostly deleted in isotype controls but could be readily observed clustering around the splenic marginal zone and T cell–B cell border of the other groups (Fig. 6, C to F). Collectively, these data indicate that CD8$^+$ T cells use a perforin-dependent cytotoxic mechanism to delete LCMV-GP–specific KL25 B cells within 3 days of infection.

CD8$^+$ T cells engage and kill LCMV-infected B cells in vivo

In several instances, we observed P14 cells juxtaposed with infected KL25 H+L B cells in splenic sections from mice 3 days after infection (fig. S2A). To visualize dynamic interactions between P14 CTLs and KL25 B cells in vivo, we generated a transgenic reporter mouse that constitutively expresses the calcium sensor protein GCaMP6s (48). Because GCaMP6s is very sensitive to changes in intracellular calcium (48), we could observe rapid signaling events after T cell–B cell engagement in vivo. Using TPM, we examined interactions between splenic mTomato$^+$ GCaMP6s$^+$ P14 cells and mCerulean$^+$ B cells 3 days after LCMV-M1 infection. Although many P14 cells fluxed calcium within the marginal zone (movie S3), presumably upon engagement of infected macrophages and other antigen-presenting cells, we also observed that P14 cells directly engage KL25 H+L B cells, undergo distinct “on/off” calcium fluxes, and follow their B cell targets (Fig. 7, A to C, and movies S3 and S4). P14 motility at this time point was very sluggish, and many cells remained essentially nonmotile, yet KL25 H+L B cells were observed migrating among P14 cells in the marginal zone and contacting them within the white pulp (Fig. 7B and movies S3 and S4). The often short-lived nature of these engagements prevented us from following a single B cell from initial engagement to death using this approach. However, we could use GCaMP6s as an in vivo cell death reporter. Cotransfer of mTomato$^+$ GCaMP6s$^+$ KL25 H+L cells and mCerulean$^+$ P14 cells allowed us to visualize KL25 H+L cells that flux calcium after P14 CTL engagement in vivo, as well as the intracellular calcium changes and rapid loss of membrane integrity associated with cell death (movie S5). Although loss of membrane integrity was rarely observed, we saw abundant KL25 cell debris both within phagocytes and extracellularly. These data indicate that LCMV-specific CTLs and B cells productively engage at early time points after infection, resulting in B cell death.

To further support CTL-mediated killing of infected LCMV-specific B cells, we generated a new recombinant LCMV-expressing codon-improved Cre recombinase (49) (r3LCMV-iCre) that we used to infect Confetti mice (50). Using combinatorial fluorescent protein expression after Cre-mediated recombination, we performed multicolor fate mapping in Confetti mice, in which all the offspring of the original Cre-expressing cells were permanently marked with a specific fluorescent protein combination. Confetti mice were injected with αIFNAR or αCD8 antibodies, infected with r3LCMV-iCre, and analyzed by confocal microscopy or TPM. Although fluorescent protein–positive cells were rare within isotype animals (fig. S2, B to D) at ~40 days after infection, αIFNAR- and CD8-depleted mice had an extensive network of infected stromal and hematopoietic cells (Fig. 7, D and F, and movie S6). However, the most notable observation was the presence of clonal clusters of IgD^{-} $GL7^{+}$ GC B cells that had previously been LCMV-infected. These infected GCs were frequently observed in the spleens and lymph nodes of αIFNAR-treated mice (Fig. 7, D and F, and movie S6). Using TPM, we observed numerous infected GC B cells within CD8-depleted mice as well (Fig. 7E and movie S6).

DISCUSSION

We have made several important observations that enhance our understanding of humoral immunity to persistent infection. First, we identified IFN-I signaling as an early negative regulator of LCMV-specific B cell survival and the subsequent production of neutralizing antibodies. IFNAR blockade enhanced the survival of both endogenous and transgenic LCMV-GP–specific B cells, resulting in accelerated development of neutralizing antibodies. Unexpectedly, IFN-I elicited its negative effects on antiviral B cells in an indirect manner by fostering the early differentiation of $CD8^{+}$ T cells into cytolytic effectors. In vivo calcium imaging studies revealed that CTLs became functionally active within the first few days of a persistent infection and acquired the ability to productively engage and kill LCMV-specific B cells in a perforin-dependent manner. IFNAR blockade rescued LCMV-specific B cells from this fate by promoting $CD8^{+}$ T cell dysfunction. In vivo fate-mapping studies in Confetti mice revealed that clonal populations of GC B cells previously infected by LCMV only emerged in the absence of IFNAR signaling or $CD8^{+}$ T cells. Collectively, these data indicate that IFN-I can play an early negative role in antiviral humoral immunity by promoting the removal of virus-specific B cell clones from the repertoire.

Early after infection, the splenic environment is hostile to LCMV-GP– specific B cells because KL25 B cells transferred into mice before infection are almost universally deleted. Some studies have suggested that CTL-mediated destruction of secondary lymphoid architecture might impair the cooperative interactions required for GC organization (26, 27, 51). However, KL25 B cells adoptively transferred into mice 1 week after infection survive, expand, and differentiate into ASCs, suggesting that destruction of lymphoid architecture does not play a major role in the impairment of LCMV-GP–specific humoral immunity. Recent reports have suggested that IFNAR blockade can accelerate viral clearance by modulating T cell activity (35, 38, 39). Our study expands upon these findings by showing that IFNAR blockade extrinsically preserves transferred and endogenous LCMV-GP B cell specificities, resulting in an accelerated neutralizing humoral response. Because serum-neutralizing activity arises several weeks after infection in IFNAR-blocked mice, this is

likely the result of GC reactions. The claim that LCMV-neutralizing B cells exist within the naïve repertoire and are deleted by $CD8^+$ T cells after infection has been debated since it was originally published (30), with the authors subsequently reporting that they were unable to reproduce their original finding (52). We uncovered no evidence for the presence of early LCMV-neutralizing specificities in the B cell repertoire; however, we did detect LCMV-GP binding clones (Fig. 2), which is in line with another published work (31). We postulate that IFNAR blockade protects LCMV-GP– specific precursors from early CTL-mediated death, allowing these cells to survive and enter GCs where they undergo extensive CD4-dependent hypermutation. This eventually drives GP-binding B cells toward LCMV-neutralizing idiotypes, similar to what is observed after HIV infection (53). This scenario would explain why $CD4^+$ T cells may be required for the enhanced viral clearance observed after IFNAR blockade (35, 38).

The predominant early anti-LCMV humoral response is directed against the nucleoprotein—an internal viral protein that would be unavailable for antibody binding. On the basis of our results, we propose a model in which BCR-mediated endocytosis by LCMV-GP–binding B cells results in their infection and subsequent killing by CTLs in a perforin-dependent manner. Planz *et al.* (30) demonstrated that NP-specific B cells are not affected by $CD8^+$ T cell depletion. This suggests that cross-presentation of LCMV antigens is insufficient and that B cells must be actively infected to be eliminated by CTLs (30). Although it remains possible that LCMV-GP–binding B cells can cross-present antigens (54) and are subsequently targeted without being infected, our data provide convincing evidence that LCMV directly infects KL25 B cells. In addition, our fate-mapping studies in r3LCMV-iCre– infected Confetti mice demonstrate clonal selection of LCMV-infected endogenous B cells in the absence of normal CTL activity (promoted by CD8 depletion or IFNAR blockade).

Our data showing early dysfunction in the virus-specific $CD8^+$ T cell response after IFNAR blockade are consistent with published disturbances in effector differentiation in the absence of “signal 3” cytokines, such as IL-12 or IFN-I (55), although it is also possible that αIFNAR drives accelerated $CD8^+$ T cell exhaustion by elevating LCMV titers early after infection. Early elevation in LCMV replication after IFNAR blockade would also explain the increased proliferation and class-switching of KL25 cells observed at day 3 after infection (Fig. 4, F and G). However, αIFNAR treatment eventually accelerates viral clearance in this model system (35, 38), and we propose that this is linked in part to improved humoral immunity.

The potency of CTL killing at early time points after infection (3 to 4 days) in our study was unexpected. The endogenous LCMV-specific CTL precursor frequency is quite low at this time, even when all specificities are considered. Nevertheless, early in vivo cytotoxic function by CTLs was reported as early as 24 to 48 hours after vaccinia virus infection (56). The high splenic antigen load, which is simultaneously available to T and B cells, fosters extensive juxtaposition of these two populations. B cells typically relocalize from the B cell zone to the T cell–B cell border after BCR engagement (41). However, the presence of abundant antigen and costimulatory signals can drive B cells away from GC fate toward terminal plasmablast differentiation (2, 57, 58). In this situation, many antigen-specific B

cells will remain near the marginal zone. During LCMV infection, nearly all early extrafollicular plasmablasts are driven toward IgG expression with coincident CXCR3 expression (2, 59, 60). Because CXCR3 ligands are known to coordinate the peripheralization of antigen-specific T cells within lymphoid follicles (61), we speculate that high-level CXCR3 ligand expression might draw LCMV-specific B cells into the same anatomical regions, increasing the risk of encountering recently generated CTLs. By generating GCaMP6s transgenic mice, we studied cell-cell contacts that gave rise to faulty antiviral humoral immunity. In vivo examination of early CTL behavior revealed both sessile and motile CTLs eliciting dynamic calcium fluxes upon engagement of neighboring B cells. We also captured examples of KL25 B cells undergoing cell death after CTL engagement. These data support the conclusion that CTLs can productively engage and kill antiviral B cells early after infection.

KL25 survival in PRF1$^{-/-}$ animals phenocopies that observed in CD8-depleted mice, indicating that CTL killing of antiviral B cells is perforin-dependent. However, CD8 depletion did not improve KL25 survival and differentiation as well as αIFNAR treatment (Fig. 6B). Although our data show that IFNAR blockade does impede early CTL differentiation and function, it is possible that αIFNAR has effects on cells other than CTLs and B cells that promote KL25 survival. Nevertheless, we propose that the difference in KL25 survival observed after αIFNAR treatment versus αCD8 treatment is best explained by the antigenic load. αIFNAR mice have more widespread splenic viral replication than observed in αCD8 or PRF1$^{-/-}$ mice (Fig. 6, D to F). This is consistent with the known antiviral properties of IFN-I and would support faster KL25 proliferation (Fig. 4F) and class switching (Fig. 4G). The bias toward CD138^{+} ASC differentiation (Fig. 6B) is also consistent with stronger antigenic stimulation (57).

One potential limitation of our study is the reliance on transgenic KL25 B cells, which have a single specificity. To broaden the relevance of our findings, we confirmed that deletion of KL25 cells is not unique to high-dose infection with LCMV-M1. Infection with LCMV-M2, which contains a lower-affinity nonneutralizing epitope (33, 62), yielded similar results (fig. S1E). We also demonstrated that IFNAR blockade protects endogenous LCMV-GP–specific B cells and accelerates the generation of neutralizing antibodies even in the absence of KL25 cells (Fig. 2). On the basis of these data, we propose that LCMV-GP– specific B cells that internalize infectious virions are likely infected and killed by CTLs early after infection. These data do not exclude the possibility that the eventual humoral immune response observed in this model is composed of at least some LCMV-GP–specific B cells that escape early infection and deletion or that emerge at later time points after infection when the CTL response subsides.

In conclusion, our data provide a clearer picture of why antiviral humoral immune responses sometimes fail during the establishment of a persistent viral infection. Although IFN-I production is crucial for viral containment, it also plays a critical role in driving the early differentiation of virus-specific CTLs. These CTLs remove a limited pool of infected antiviral B cell clones. Interference with IFN-I signaling might temporarily increase viral loads, but it also preserves antiviral B cell clones by promoting CTL dysfunction. Some of these clones eventually enter GCs and serve as raw material for somatic hypermutation and

accelerated acquisition of serum-neutralizing activity. Understanding the prevalence of virus-specific B cell infection and death may guide new immunization strategies. Our findings also suggest that IFNAR blockade might be a useful strategy for promoting endogenous B cell survival and improving neutralizing antibody responses after virus infection.

MATERIALS AND METHODS

Mice

C57BL/6J (B6), B6.129(Cg)-Gt(ROSA)26Sor$^{tm4(ACTB-tdTomato,-EGFP)Luo}$/J (mTomato), C57BL/6-Tg(TcraTcrb)1100Mjb/J (OT-I), C57BL/6-Prf1^{tm1Sdz}/J (PRF$^{-/-}$), and Gt(ROSA)26Sor$^{tm1(CAG-Brainbow2.1)Cle}$/J (Confetti) mice were purchased from the Jackson Laboratory. Blimp1-YFP (provided by M. Nussenzweig, Rockefeller University), actin-mCerulean, actin-mOrange, actin-YFP, IFNAR$^{-/-}$ (provided by J. Sprent, formerly at the Scripps Research Institute), KL25 H (provided by H. Hengartner, University of Zurich), KL25 H+L (provided by M. Iannacone, San Raffaele Scientific Institute), VI10YEN, P14, Thy1.1^{+} P14, SMARTA, mCerulean^{+} SMARTA, and mOrange^{+} SMARTA (all on a pure B6 background) were bred and maintained under specific pathogen–free conditions at the National Institutes of Health (NIH). The KL25 H+L mice were originally generated by P. Greenberg at the University of Washington. All mice in this study were handled in accordance with the guidelines set forth by the NIH Animal Care and Use Committee.

Transgenic mouse generation

INS2-CMV-β-ac-GCaMP6s transgenic mice (actin-GCaMP6s) were generated at the National Institute of Mental Health (NIMH) Transgenic Core Facility. The construct was prepared for microinjection into the pronuclei of fertilized C57BL/6J mouse eggs. After selection of transgene-positive founder lines, all mice were backcrossed one additional generation onto the C57BL/6J background before they were intercrossed.

Generation of r3LCMV-iCre

Virus rescue was performed as described previously (63).

Virus infection

Mice were infected intravenously with 2.5×10^6 PFU of LCMV CL13, LCMV CL13 M1 (33), or LCMV CL13 M2 (33). An acute infection was generated by infecting mice with low-dose (4×10^4 PFU) LCMV CL13 M1. r3LCMV-iCre infections were achieved by intravenous injection of 3×10^4 PFU.

Splenocyte enumeration and flow cytometry

Spleens from infected animals were dissociated, and single-cell suspensions were stained with the following antibodies from BioLegend: anti-GL7, anti-CD138, anti-CD19, anti-CD45.1, anti-CD8, anti-CD4, anti-Thy1.1, anti-Thy1.2, anti-CD11c, anti-CD11b, and anti-IgM. 7-Aminoactinomycin D and counting beads (Flow Cytometry Absolute Count Standard) were added to each sample before acquisition to allow calculation of cells per

sample. Intracellular cytokine staining was performed by standard methods, staining intracellularly with anti–IFN-γ and anti-TNFα (BioLegend). Intracellular granzyme B and LCMV were detected using anti–granzyme B or anti-LCMV antibodies, respectively. Samples were acquired using an LSR II digital flow cytometer (BD Biosciences), and data were analyzed using FlowJo software version 10.0.7 (Tree Star).

Isolation of naïve B cells and CD8$^+$ T cells

Naïve B cells or CD8 T cells were isolated from single-cell suspensions of naïve WT or transgenic lymphocytes using a mouse B cell negative selection kit or a mouse CD8$^+$ T cell negative selection kit, respectively (STEMCELL Technologies). The purity of the cells after isolation was determined to be greater than 95%.

In vivo depletion studies

All antibodies used for cell depletion and blocking assays were purchased from BioXCell. One milligram of anti-IFNAR (MAR1-5A3) and 200 μl of clodronate liposomes (Encapsula NanoSciences) were injected intravenously on days −1 and +2 after infection.

Enzyme-linked immunosorbent assay

LCMV-specific antibodies were quantified using the Amplex ELISA Development Kit for Mouse IgG (Invitrogen). Flat-bottom plates were coated with purified LCMV or LCMV-GP-Fc. Plates were blocked and incubated with hybridoma supernatant. Plates were then washed and incubated with goat anti-mouse IgG horseradish peroxidase followed by Amplex reaction mixture for 30 min.

Hybridomas

Hybridomas were generated using the ClonaCell-HY Hybridoma Kit (STEMCELL Technologies).

Immunohistochemistry

Spleens were fixed in 2.5% buffered formalin overnight, equilibrated in a 30% sucrose solution for 2 to 4 hours, and embedded in tissue freezing medium (Triangle Biomedical Sciences). Cryosections (20 to 30 μm) were cut using a Leica CM1850 cryostat. Images were acquired using an Olympus FV1200 laser scanning confocal microscope equipped with four detectors and six laser lines (405, 458, 488, 515, 559, and 635 nm).

Neutralizing antibody assay

Twofold serial dilutions of serum (12 μl) were incubated with ~40 to 50 focus-forming units of LCMV-CL13 or LCMV-M1 in 96-well round-bottom plates for 90 min at 37°C in a 5% CO_2 incubator. After the incubation, 2.5×10^4 Vero cells were added to each well. After ~4 hours, the liquid in each well was replaced with 0.75% methylcellulose in Dulbecco's modified Eagle's medium incubated for 44 to 48 hours at 37°C in a 5% CO_2 incubator. Cells were subsequently fixed and stained for LCMV antigen as described previously (64). Neutralizing antibody titers were determined as 50% inhibition.

In vitro cytokine production

A total of 5×10^5 P14 $CD8^+$ T cell–containing splenocytes from mice at days 3 to 4 after infection were plated in 96-well round-bottom plates in RPMI complete medium with brefeldin A (5 μg/ml; Sigma) at 37°C for 5 hours with or without $GP_{33–41}$ peptide (KAVYNFATC; 2 μg/ml; AnaSpec).

In vitro CTL activity

$Thy1.1^+$ P14 T cells from mice at days 3 to 4 after infection were isolated and mixed (at a ratio of 1:1; 75,000 of each) with Cell Tracker Violet (CTV; Invitrogen)–labeled peptide-pulsed splenocyte targets and cocultured in RPMI complete medium. Specific lysis was calculated as follows: (non–peptide-pulsed: peptide-pulsed without CTLs)/(non–peptide-pulsed: peptide-pulsed with CTLs) × 100.

Adoptive transfers

For late transfer imaging studies, 1000 to 5000 naïve purified OFP^+ $CD4^+$ SMARTA T cells and 1×10^6 to 2×10^6 $mCerulean^+$ Blimp1-YFP^+ KL25 H cells were injected intravenously into day 6 LCMV-M1– infected B6 mice. For imaging and fluorescence-activated cell sorting (FACS) analysis of day 7 isotype control–treated versus αIFNAR antibody–treated mice, 1×10^6 to 2×10^6 $mCerulean^+$ Blimp1-YFP^+ KL25 H cells were injected intravenously into B6 mice 1 day before intravenous LCMV-M1 infection. In vivo calcium imaging studies were set up by seeding B6 mice intravenously with 50,000 $mTomato^+$ $GCaMP6s^+$ P14 and 1×10^6 $mCerulean^+$ KL25 H+L cells or with 50,000 $mCerulean^+$ P14 and 2.5×10^6 $mTomato^+$ $GCaMP6s^+$ KL25 H+L cells. All recipient mice were infected with LCMV-M1 1 day later.

Two-photon microscopy

Two-photon imaging was performed as described previously (65).

Statistical analysis

Statistical significance ($P < 0.05$) was determined using Student's t test (two groups) or one-way analysis of variance (ANOVA; more than two groups). ANOVA on ranks was used for data sets with a non-Gaussian distribution and more than two groups. All statistical analyses were performed using GraphPad Prism 6.0 or SigmaPlot 11.0.

Data deposition and materials availability

All new mice and reagents generated in this study will be made available to other investigators. GCaMP6s transgenic mice will be available under a standard NIH model organism material transfer agreement.

Supplementary Material

Refer to Web version on PubMed Central for supplementary material.

Acknowledgments

We would like to thank J. Pickel and the NIMH Transgenic Core Facility for their assistance in generating the new transgenic GCaMP6s reporter mice. We also want to acknowledge D. Maric and the National Institute of Neurological Disorders and Stroke Sorting Facility for assistance.

Funding: This research was supported by the intramural program at the NIH.

REFERENCES AND NOTES

1. Victora GD, Nussenzweig MC. Germinal centers. Annu. Rev. Immunol. 2012; 30:429–457. [PubMed: 22224772]
2. Nutt SL, Hodgkin PD, Tarlinton DM, Corcoran LM. The generation of antibody-secreting plasma cells. Nat. Rev. Immunol. 2015; 15:160–171. [PubMed: 25698678]
3. Baumjohann D, Preite S, Reboldi A, Ronchi F, Ansel KM, Lanzavecchia A, Sallusto F. Persistent antigen and germinal center B cells sustain T follicular helper cell responses and phenotype. Immunity. 2013; 38:596–605. [PubMed: 23499493]
4. Welsh RM, Selin LK, Szomolanyi-Tsuda E. Immunological memory to viral infections. Annu. Rev. Immunol. 2004; 22:711–743. [PubMed: 15032594]
5. Virgin HW, Wherry EJ, Ahmed R. Redefining chronic viral infection. Cell. 2009; 138:30–50. [PubMed: 19596234]
6. Andersen C, Jensen T, Nansen A, Marker O, Thomsen AR. $CD4^+$ T cell-mediated protection against a lethal outcome of systemic infection with vesicular stomatitis virus requires CD40 ligand expression, but not IFN-γ or IL-4. Int. Immunol. 1999; 11:2035–2042. [PubMed: 10590269]
7. Edelmann KH, Wilson CB. Role of CD28/CD80-86 and CD40/CD154 costimulatory interactions in host defense to primary herpes simplex virus infection. J. Virol. 2001; 75:612–621. [PubMed: 11134274]
8. Graham MB, Braciale TJ. Resistance to and recovery from lethal influenza virus infection in B lymphocyte-deficient mice. J. Exp. Med. 1997; 186:2063–2068. [PubMed: 9396777]
9. Whitmire JK, Slifka MK, Grewal IS, Flavell RA, Ahmed R. CD40 ligand-deficient mice generate a normal primary cytotoxic T-lymphocyte response but a defective humoral response to a viral infection. J. Virol. 1996; 70:8375–8381. [PubMed: 8970958]
10. Rehermann B, Ferrari C, Pasquinelli C, Chisari FV. The hepatitis B virus persists for decades after patients' recovery from acute viral hepatitis despite active maintenance of a cytotoxic T-lymphocyte response. Nat. Med. 1996; 2:1104–1108. [PubMed: 8837608]
11. Logvinoff C, Major ME, Oldach D, Heyward S, Talal A, Balfe P, Feinstone SM, Alter H, Rice CM, McKeating JA. Neutralizing antibody response during acute and chronic hepatitis C virus infection. Proc. Natl. Acad. Sci. U.S.A. 2004; 101:10149–10154. [PubMed: 15220475]
12. Mouquet H. Antibody B cell responses in HIV-1 infection. Trends Immunol. 2014; 35:549–561. [PubMed: 25240985]
13. Hangartner L, Zinkernagel RM, Hengartner H. Antiviral antibody responses: The two extremes of a wide spectrum. Nat. Rev. Immunol. 2006; 6:231–243. [PubMed: 16498452]
14. Ahmed R, Oldstone MB. Organ-specific selection of viral variants during chronic infection. J. Exp. Med. 1988; 167:1719–1724. [PubMed: 3367096]
15. Bergthaler A, Flatz L, Hegazy AN, Johnson S, Horvath E, Löhning M, Pinschewer DD. Viral replicative capacity is the primary determinant of lymphocytic choriomeningitis virus persistence and immunosuppression. Proc. Natl. Acad. Sci. U.S.A. 2010; 107:21641–21646. [PubMed: 21098292]
16. Sullivan BM, Emonet SF, Welch MJ, Lee AM, Campbell KP, de la Torre JC, Oldstone MB. Point mutation in the glycoprotein of lymphocytic choriomeningitis virus is necessary for receptor binding, dendritic cell infection, and long-term persistence. Proc. Natl. Acad. Sci. U.S.A. 2011; 108:2969–2974. [PubMed: 21270335]
17. Oldstone MBA. Biology and pathogenesis of lymphocytic choriomeningitis virus infection. Curr. Top. Microbiol. Immunol. 2002; 263:83–117. [PubMed: 11987822]

18. Slifka MK. Mechanisms of humoral immunity explored through studies of LCMV infection. Curr. Top. Microbiol. Immunol. 2002; 263:67–81. [PubMed: 11987820]
19. Oliviero B, Cerino A, Varchetta S, Paudice E, Pai S, Ludovisi S, Zaramella M, Michelone G, Pugnale P, Negro F, Barnaba V, Mondelli MU. Enhanced B-cell differentiation and reduced proliferative capacity in chronic hepatitis C and chronic hepatitis B virus infections. J. Hepatol. 2011; 55:53–60. [PubMed: 21145853]
20. Moir S, Fauci AS. B cells in HIV infection and disease. Nat. Rev. Immunol. 2009; 9:235–245. [PubMed: 19319142]
21. Roughan JE, Reardon KM, Cogburn KE, Quendler H, Pockros PJ, Law M. Chronic hepatitis C virus infection breaks tolerance and drives polyclonal expansion of autoreactive B cells. Clin. Vaccine Immunol. 2012; 19:1027–1037. [PubMed: 22623650]
22. Hangartner L, Zellweger RM, Giobbi M, Weber J, Eschli B, Mccoy KD, Harris N, Recher M, Zinkernagel RM, Hengartner H. Nonneutralizing antibodies binding to the surface glycoprotein of lymphocytic choriomeningitis virus reduce early virus spread. J. Exp. Med. 2006; 203:2033–2042. [PubMed: 16880253]
23. Bergthaler A, Flatz L, Verschoor A, Hegazy AN, Holdener M, Fink K, Eschli B, Merkler D, Sommerstein R, Horvath E, Fernandez M, Fitsche A, Senn BM, Verbeek JS, Odermatt B, Siegrist C-A, Pinschewer DD. Impaired antibody response causes persistence of prototypic T cell-contained virus. PLOS Biol. 2009; 7:e1000080. [PubMed: 19355789]
24. Masopust D, Murali-Krishna K, Ahmed R. Quantitating the magnitude of the lymphocytic choriomeningitis virus-specific CD8 T-cell response: It is even bigger than we thought. J. Virol. 2007; 81:2002–2011. [PubMed: 17151096]
25. McDermott DS, Varga SM. Quantifying antigen-specific CD4 T cells during a viral infection: CD4 T cell responses are larger than we think. J. Immunol. 2011; 187:5568–5576. [PubMed: 22043009]
26. Mueller SN, Matloubian M, Clemens DM, Sharpe AH, Freeman GJ, Gangappa S, Larsen CP, Ahmed R. Viral targeting of fibroblastic reticular cells contributes to immunosuppression and persistence during chronic infection. Proc. Natl. Acad. Sci. U.S.A. 2007; 104:15430–15435. [PubMed: 17878315]
27. Mueller SN, Hosiawa-Meagher KA, Konieczny BT, Sullivan BM, Bachmann MF, Locksley RM, Ahmed R, Matloubian M. Regulation of homeostatic chemokine expression and cell trafficking during immune responses. Science. 2007; 317:670–674. [PubMed: 17673664]
28. Recher M, Lang KS, Hunziker L, Freigang S, Eschli B, Harris NL, Navarini A, Senn BM, Fink K, Lötscher M, Hangartner L, Zellweger R, Hersberger M, Theocharides A, Hengartner H, Zinkernagel RM. Deliberate removal of T cell help improves virus-neutralizing antibody production. Nat. Immunol. 2004; 5:934–942. [PubMed: 15300247]
29. Pinschewer DD, Perez M, Jeetendra E, Bächi T, Horvath E, Hengartner H, Whitt MA, de la Torre JC, Zinkernagel RM. Kinetics of protective antibodies are determined by the viral surface antigen. J. Clin. Invest. 2004; 114:988–993. [PubMed: 15467838]
30. Planz O, Seiler P, Hengartner H, Zinkernagel RM. Specific cytotoxic T cells eliminate B cells producing virus-neutralizing antibodies [corrected]. Nature. 1996; 382:726–729. [PubMed: 8751445]
31. Eschli B, Zellweger RM, Wepf A, Lang KS, Quirin K, Weber J, Zinkernagel RM, Hengartner H. Early antibodies specific for the neutralizing epitope on the receptor binding subunit of the lymphocytic choriomeningitis virus glycoprotein fail to neutralize the virus. J. Virol. 2007; 81:11650–11657. [PubMed: 17699567]
32. Hangartner L, Senn BM, Ledermann B, Kalinke U, Seiler P, Bucher E, Zellweger RM, Fink K, Odermatt B, Bürki K, Zinkernagel RM, Hengartner H. Antiviral immune responses in gene-targeted mice expressing the immunoglobulin heavy chain of virus-neutralizing antibodies. Proc. Natl. Acad. Sci. U.S.A. 2003; 100:12883–12888. [PubMed: 14569006]
33. Osokine I, Snell LM, Cunningham CR, Yamada DH, Wilson EB, Elsaesser HJ, de la Torre JC, Brooks D. Type I interferon suppresses de novo virus-specific CD4 Th1 immunity during an established persistent viral infection. Proc. Natl. Acad. Sci. U.S.A. 2014; 111:7409–7414. [PubMed: 24799699]

34. Zellweger RM, Hangartner L, Weber J, Zinkernagel RM, Hengartner H. Parameters governing exhaustion of rare T cell-independent neutralizing IgM-producing B cells after LCMV infection. Eur. J. Immunol. 2006; 36:3175–3185. [PubMed: 17125146]
35. Teijaro JR, Ng C, Lee AM, Sullivan BM, Sheehan KCF, Welch M, Schreiber RD, de la Torre JC, Oldstone MBA. Persistent LCMV infection is controlled by blockade of type I interferon signaling. Science. 2013; 340:207–211. [PubMed: 23580529]
36. Bolen CR, Robek MD, Brodsky L, Schulz V, Lim JK, Taylor MW, Kleinstein SH. The blood transcriptional signature of chronic hepatitis C virus is consistent with an ongoing interferon-mediated antiviral response. J. Interferon Cytokine Res. 2013; 33:15–23. [PubMed: 23067362]
37. Doyle T, Goujon C, Malim MH. HIV-1 and interferons: Who's interfering with whom? Nat. Rev. Microbiol. 2015; 13:403–413. [PubMed: 25915633]
38. Wilson EB, Yamada DH, Elsaesser H, Herskovitz J, Deng J, Cheng G, Aronow BJ, Karp CL, Brooks DG. Blockade of chronic type I interferon signaling to control persistent LCMV infection. Science. 2013; 340:202–207. [PubMed: 23580528]
39. Ng CT, Sullivan BM, Teijaro JR, Lee AM, Welch M, Rice S, Sheehan KCF, Schreiber RD, Oldstone MBA. Blockade of interferon beta, but not interferon alpha, signaling controls persistent viral infection. Cell Host Microbe. 2015; 17:653–661. [PubMed: 25974304]
40. Fink K, Lang KS, Manjarrez-Orduno N, Junt T, Senn BM, Holdener M, Akira S, Zinkernagel RM, Hengartner H. Early type I interferon-mediated signals on B cells specifically enhance antiviral humoral responses. Eur. J. Immunol. 2006; 36:2094–2105. [PubMed: 16810635]
41. Junt T, Moseman EA, Iannacone M, Massberg S, Lang PA, Boes M, Fink K, Henrickson SE, Shayakhmetov DM, Di Paolo NC, van Rooijen N, Mempel TR, Whelan SP, von Andrian UH. Subcapsular sinus macrophages in lymph nodes clear lymph-borne viruses and present them to antiviral B cells. Nature. 2007; 450:110–114. [PubMed: 17934446]
42. Seiler P, Aichele P, Odermatt B, Hengartner H, Zinkernagel RM, Schwendener RA. Crucial role of marginal zone macrophages and marginal zone metallophils in the clearance of lymphocytic choriomeningitis virus infection. Eur. J. Immunol. 1997; 27:2626–2633. [PubMed: 9368619]
43. Müller S, Hunziker L, Enzler S, Bühler-Jungo M, Di Santo JP, Zinkernagel RM, Mueller C. Role of an intact splenic microarchitecture in early lymphocytic choriomeningitis virus production. J. Virol. 2002; 76:2375–2383. [PubMed: 11836415]
44. Fahey LM, Wilson EB, Elsaesser H, Fistonich CD, McGavern DB, Brooks DG. Viral persistence redirects CD4 T cell differentiation toward T follicular helper cells. J. Exp. Med. 2011; 208:987–999. [PubMed: 21536743]
45. Hogquist KA, Jameson SC, Heath WR, Howard JL, Bevan MJ, Carbone FR. T cell receptor antagonist peptides induce positive selection. Cell. 1994; 76:17–27. [PubMed: 8287475]
46. Curtsinger JM, Mescher MF. Inflammatory cytokines as a third signal for T cell activation. Curr. Opin. Immunol. 2010; 22:333–340. [PubMed: 20363604]
47. Pircher H, Bürki K, Lang R, Hengartner H, Zinkernagel RM. Tolerance induction in double specific T-cell receptor transgenic mice varies with antigen. Nature. 1989; 342:559–561. [PubMed: 2573841]
48. Chen T-W, Wardill TJ, Sun Y, Pulver SR, Renninger SL, Baohan A, Schreiter ER, Kerr RA, Orger MB, Jayaraman V, Looger LL, Svoboda K, Kim DS. Ultrasensitive fluorescent proteins for imaging neuronal activity. Nature. 2013; 499:295–300. [PubMed: 23868258]
49. Shimshek DR, Kim J, Hübner MR, Spergel DJ, Buchholz F, Casanova E, Stewart AF, Seeburg PH, Sprengel R. Codon-improved Cre recombinase (iCre) expression in the mouse. Genesis. 2002; 32:19–26. [PubMed: 11835670]
50. Snippert HJ, van der Flier LG, Sato T, van Es JH, van den Born M, Kroon-Veenboer C, Barker N, Klein AM, van Rheenen J, Simons BD, Clevers H. Intestinal crypt homeostasis results from neutral competition between symmetrically dividing Lgr5 stem cells. Cell. 2010; 143:134–144. [PubMed: 20887898]
51. Leist TP, Rüedi E, Zinkernagel RM. Virus-triggered immune suppression in mice caused by virus-specific cytotoxic T cells. J. Exp. Med. 1988; 167:1749–1754. [PubMed: 2966846]
52. Planz O, Seiler P, Hengartner H, Zinkernagel RM. Specific cytotoxic T cells eliminate cells producing neutralizing antibodies. Nature. 2003; 426:474. [PubMed: 14647387]

53. Wu X, Zhou T, Zhu J, Zhang B, Georgiev I, Wang C, Chen X, Longo NS, Louder M, McKee K, O'Dell S, Perfetto S, Schmidt SD, Shi W, Wu L, Yang Y, Yang Z-Y, Yang Z, Zhang Z, Bonsignori M, Crump JA, Kapiga SH, Sam NE, Haynes BF, Simek M, Burton DR, Koff WC, Doria-Rose NA, Connors M, NISC Comparative Sequencing Program. Mullikin JC, Nabel GJ, Roederer M, Shapiro L, Kwong PD, Mascola JR. Focused evolution of HIV-1 neutralizing antibodies revealed by structures and deep sequencing. Science. 2011; 333:1593–1602. [PubMed: 21835983]
54. Robson NC, Donachie AM, Mowat AM. Simultaneous presentation and cross-presentation of immune-stimulating complex-associated cognate antigen by antigen-specific B cells. Eur. J. Immunol. 2008; 38:1238–1246. [PubMed: 18398931]
55. Mescher MF, Curtsinger JM, Agarwal P, Casey KA, Gerner M, Hammerbeck CD, Popescu F, Xiao Z. Signals required for programming effector and memory development by CD8+ T cells. Immunol. Rev. 2006; 211:81–92. [PubMed: 16824119]
56. Chiu C, Heaps AG, Cerundolo V, McMichael AJ, Bangham CR, Callan MFC. Early acquisition of cytolytic function and transcriptional changes in a primary $CD8^+$ T-cell response in vivo. Blood. 2007; 109:1086–1094. [PubMed: 16990607]
57. Paus D, Phan TG, Chan TD, Gardam S, Basten A, Brink R. Antigen recognition strength regulates the choice between extrafollicular plasma cell and germinal center B cell differentiation. J. Exp. Med. 2006; 203:1081–1091. [PubMed: 16606676]
58. Fink K, Manjarrez-Orduño N, Schildknecht A, Weber J, Senn BM, Zinkernagel RM, Hengartner H. B cell activation state-governed formation of germinal centers following viral infection. J. Immunol. 2007; 179:5877–5885. [PubMed: 17947661]
59. Kunkel EJ, Butcher EC. Plasma-cell homing. Nat. Rev. Immunol. 2003; 3:822–829. [PubMed: 14523388]
60. Hauser AE, Debes GF, Arce S, Cassese G, Hamann A, Radbruch A, Manz RA. Chemotactic responsiveness toward ligands for CXCR3 and CXCR4 is regulated on plasma blasts during the time course of a memory immune response. J. Immunol. 2002; 169:1277–1282. [PubMed: 12133949]
61. Sung JH, Zhang H, Moseman EA, Alvarez D, Iannacone M, Henrickson SE, de la Torre JC, Groom JR, Luster AD, von Andrian UH. Chemokine guidance of central memory T cells is critical for antiviral recall responses in lymph nodes. Cell. 2012; 150:1249–1263. [PubMed: 22980984]
62. Yamada DH, Elsaesser H, Lux A, Timmerman JM, Morrison SL, de la Torre JC, Nimmerjahn F, Brooks DG. Suppression of Fcγ-receptor-mediated antibody effector function during persistent viral infection. Immunity. 2015; 42:379–390. [PubMed: 25680277]
63. Emonet SF, Garidou L, McGavern DB, de la Torre JC. Generation of recombinant lymphocytic choriomeningitis viruses with trisegmented genomes stably expressing two additional genes of interest. Proc. Natl. Acad. Sci. U.S.A. 2009; 106:3473–3478. [PubMed: 19208813]
64. Battegay M, Cooper S, Althage A, Bänziger J, Hengartner H, Zinkernagel RM. Quantification of lymphocytic choriomeningitis virus with an immunological focus assay in 24- or 96-well plates. J. Virol. Methods. 1991; 33:191–198. [PubMed: 1939506]
65. Zinselmeyer BH, Heydari S, Sacristán C, Nayak D, Cammer M, Herz J, Cheng X, Davis SJ, Dustin ML, McGavern DB. PD-1 promotes immune exhaustion by inducing antiviral T cell motility paralysis. J. Exp. Med. 2013; 210:757–774. [PubMed: 23530125]
66. Muzumdar MD, Tasic B, Miyamichi K, Li L, Luo L. A global double-fluorescent Cre reporter mouse. Genesis. 2007; 45:593–605. [PubMed: 17868096]
67. Kägi D, Ledermann B, Bürki K, Seiler P, Odermatt B, Olsen KJ, Podack ER, Zinkernagel RM, Hengartner H. Cytotoxicity mediated by T cells and natural killer cells is greatly impaired in perforin-deficient mice. Nature. 1994; 369:31–37. [PubMed: 8164737]
68. Fooksman DR, Schwickert TA, Victora GD, Dustin ML, Nussenzweig MC, Skokos D. Development and migration of plasma cells in the mouse lymph node. Immunity. 2010; 33:118–127. [PubMed: 20619695]
69. Gossa S, Nayak D, Zinselmeyer BH, McGavern DB. Development of an immunologically tolerated combination of fluorescent proteins for in vivo two-photon imaging. Sci. Rep. 2014; 4:6664. [PubMed: 25322934]

70. Muller U, Steinhoff U, Reis LF, Hemmi S, Pavlovic J, Zinkernagel RM, Aguet M. Functional role of type I and type II interferons in antiviral defense. Science. 1994; 264:1918–1921. [PubMed: 8009221]

71. Oxenius A, Bachmann MF, Zinkernagel RM, Hengartner H. Virus-specific MHC-class II-restricted TCR-transgenic mice: Effects on humoral and cellular immune responses after viral infection. Eur. J. Immunol. 1998; 28:390–400. [PubMed: 9485218]

72. Devlin EE, Dacosta L, Mohandas N, Elliott G, Bodine DM. A transgenic mouse model demonstrates a dominant negative effect of a point mutation in the RPS19 gene associated with Diamond-Blackfan anemia. Blood. 2010; 116:2826–2835. [PubMed: 20606162]

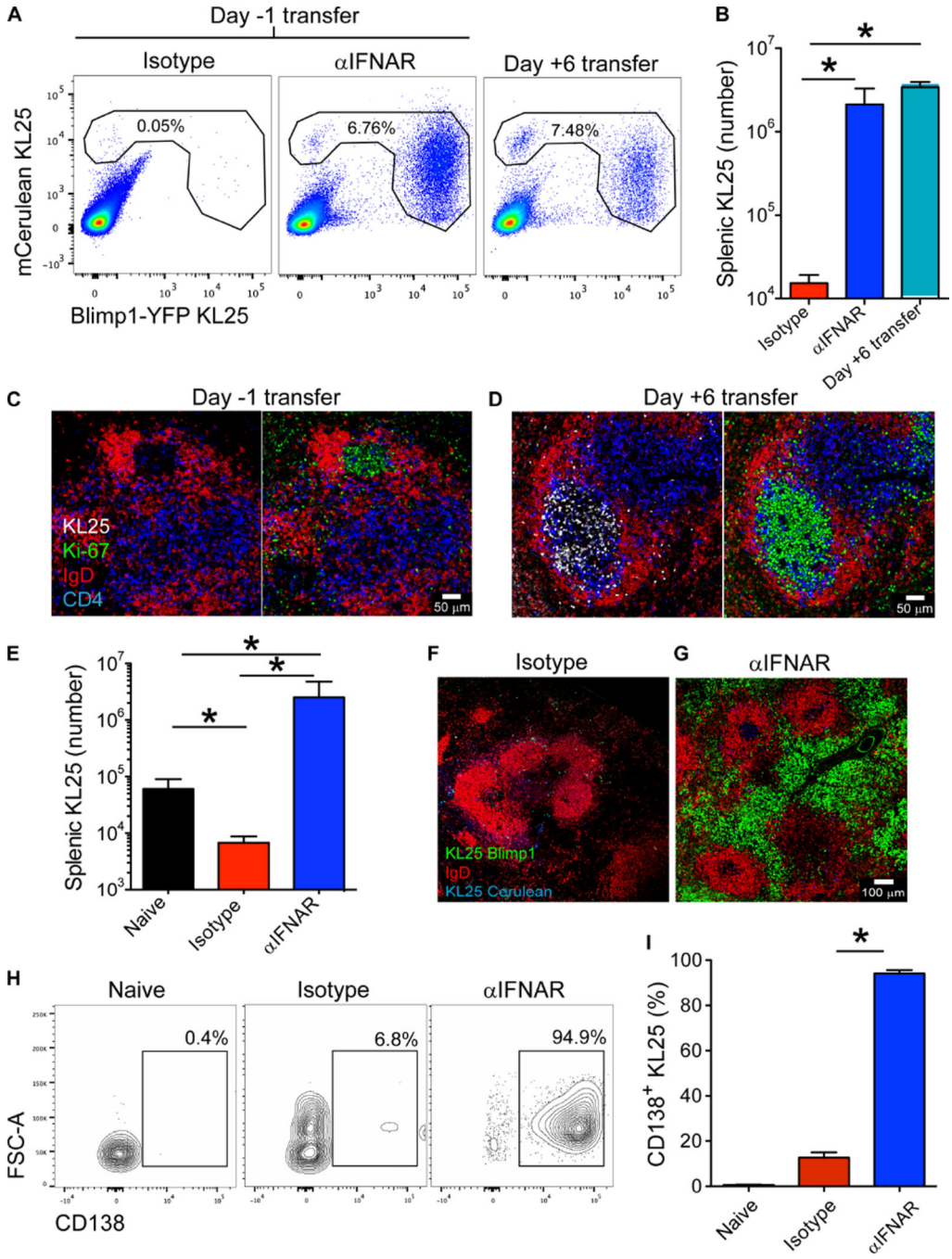

Fig. 1. LCMV-specific B cells are deleted after infection

(**A**) Representative FACS plots showing the percentages of KL25 B cells within splenic B cells (gated on B lineage cells; those expressing either CD19 or CD138) from LCMV-M1–infected mice. KL25 cells were transferred into isotype and αIFNAR animals 1 day before infection. KL25 cells were transferred into “late transfer” animals 6 days after infection. (**B**) Quantification of splenic KL25 numbers from isotype, αIFNAR, and late transfer mice shown in (A) ($n = 4$ mice per group; two independent experiments; $*P < 0.05$). (**C** and **D**) Splenic images depicting the distribution of KL25 B cells (white) after adoptive transfer into

LCMV-M1–infected mice on day −1 (C) or day +6 (D). Spleens were harvested at day 14 after transfer and stained with antibodies against IgD (red), Ki67 (green), and CD4 (blue). Note the presence of proliferating Ki67$^+$ KL25 cells in GCs after late transfer (n = 3 mice per group; two independent experiments). (**E**) Splenic KL25 numbers from naïve, isotype, and αIFNAR recipients at 7 days after infection (n = 4 mice per group; 23 independent experiments; *P < 0.05). (**F** and **G**) Splenic micrographs of mCerulean$^+$ (blue) Blimp1-YFP$^+$ (green) KL25 cells in isotype versus αIFNAR recipients at 7 days after infection stained with IgD (red) (n = 3 mice per group; five independent experiments). (**H**) Representative FACS plots of splenic mCerulean$^+$ KL25 cells from naïve versus day 7 LCMV-M1– infected (isotype versus αIFNAR) mice depicting the frequency of CD138$^+$ ASCs (gated on B lineage cells; those expressing either CD19 or CD138 and mCerulean). FSC-A, Forward Scatter-Area. (**I**) Quantification of CD138$^+$ KL25 frequency from naïve, isotype, and αIFNAR mice showing (H) (n = 4 to 5 mice per group; 18 independent experiments; *P < 0.05). For all bar graphs, data are means + SD.

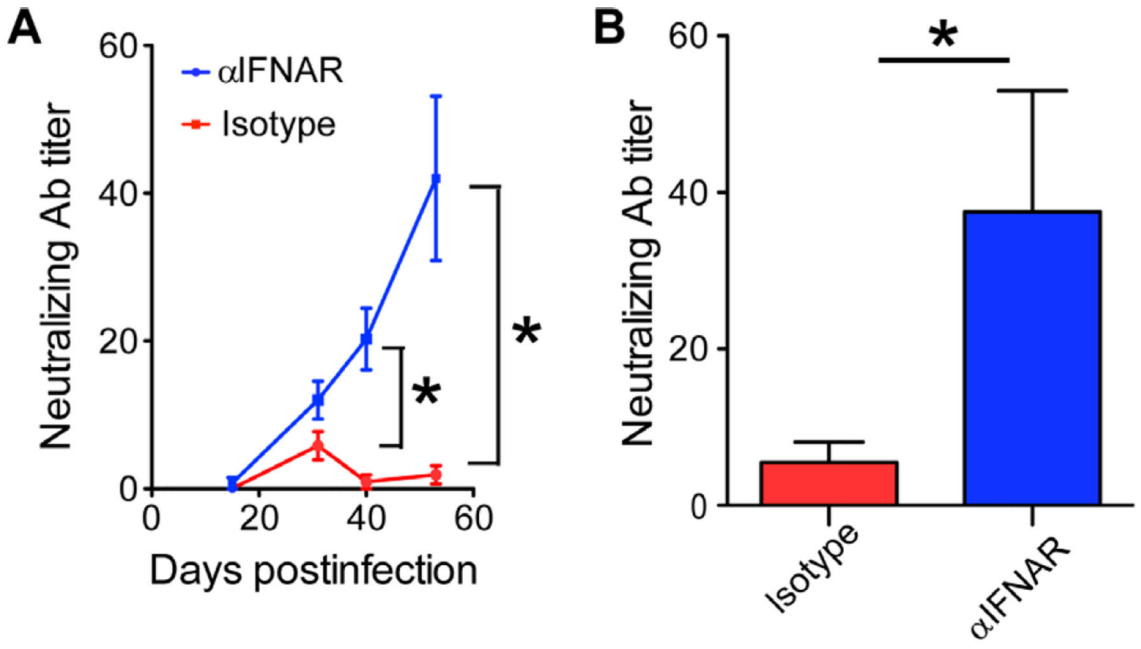

C

Condition	Total hybridomas	LCMV binding	GP binding
Isotype	60	10 (16%)	4 (6.6%)
αIFNAR	360	78 (21.1%)	43 (13.3%)

Fig. 2. IFN-I signaling mediates deletion of endogenous LCMV-GP–specific B cells

(**A**). Serum-neutralizing antibody (Ab) titers from LCMV-M1–infected isotype or αIFNAR-blocked animals ($n = 5$ mice per group; two independent experiments; $*P < 0.05$). (**B**) Serum-neutralizing Ab titers from WT LCMV-CL13 isotype versus αIFNAR mice 200 days after infection ($n = 5$ mice per group; $*P < 0.05$). (**C**) Summary of hybridoma generation and reactivities from isotype versus αIFNAR LCMV-infected spleens. For all plots, data are means + SD.

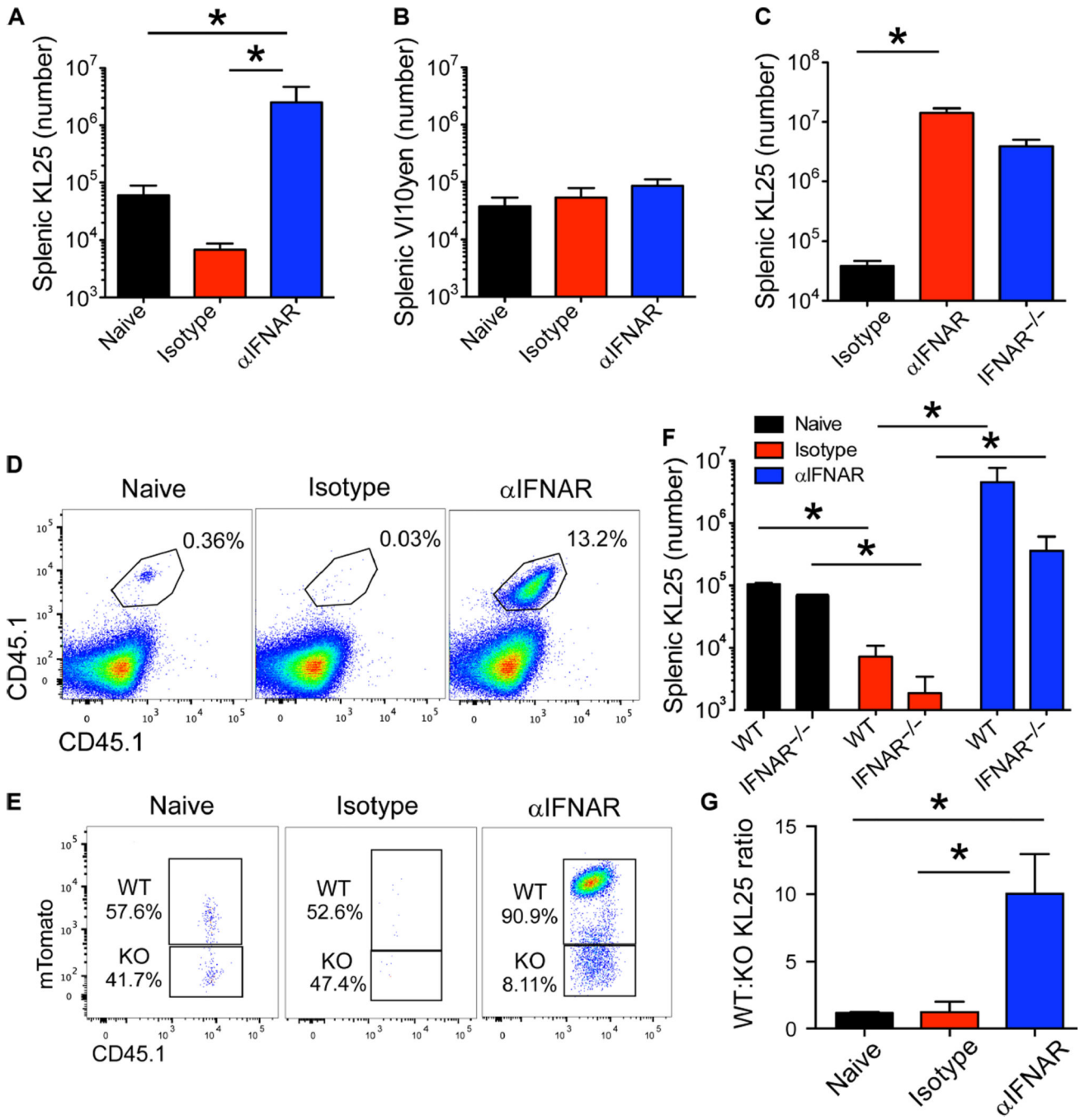

Fig. 3. Deletion of LCMV-GP–specific B cells is antigen-specific and dependent on extrinsic IFNAR signaling

(**A** and **B**) Splenic counts of cotransferred KL25 (A) and VI10YEN (B) B cells at day 7 after infection of isotype versus αIFNARmice. Cotransfer into uninfected B6 mice served as a control for this experiment ($n = 4$ to 5 mice per group; three independent experiments; $*P < 0.05$). (**C**) Splenic KL25 counts from isotype, αIFNAR, or IFNAR-deficient mice at 7 days after LCMV-M1 infection ($n = 4$ mice per group; two independent experiments; $*P < 0.05$). (**D** and **E**) Representative plots of competitive WT ($CD45.1^+$ $mTomato^+$) versus $IFNAR^{-/-}$

(CD45.1$^+$) KL25 B cells in naïve, isotype, and αIFNAR recipients 7 days after LCMV-M1 infection (gated on B lineage cells; those expressing either CD19 or CD138). KO, knockout. (**F**) Splenic KL25 counts of WT versus IFNAR$^{-/-}$ KL25 cells in naïve, isotype, and αIFNAR recipients 7 days after infection. Quantification of FACS data in (D) and (E) (n = 4 to 5 mice per group; two independent experiments; *P < 0.05). (**G**) Ratio of WT to IFNAR$^{-/-}$ KL25 cells in naïve, isotype, and αIFNAR recipients 7 days after infection. Ratio calculated from the data in (E) (n = 4mice per group; two independent experiments; *P < 0.05). For all plots, data are means + SD.

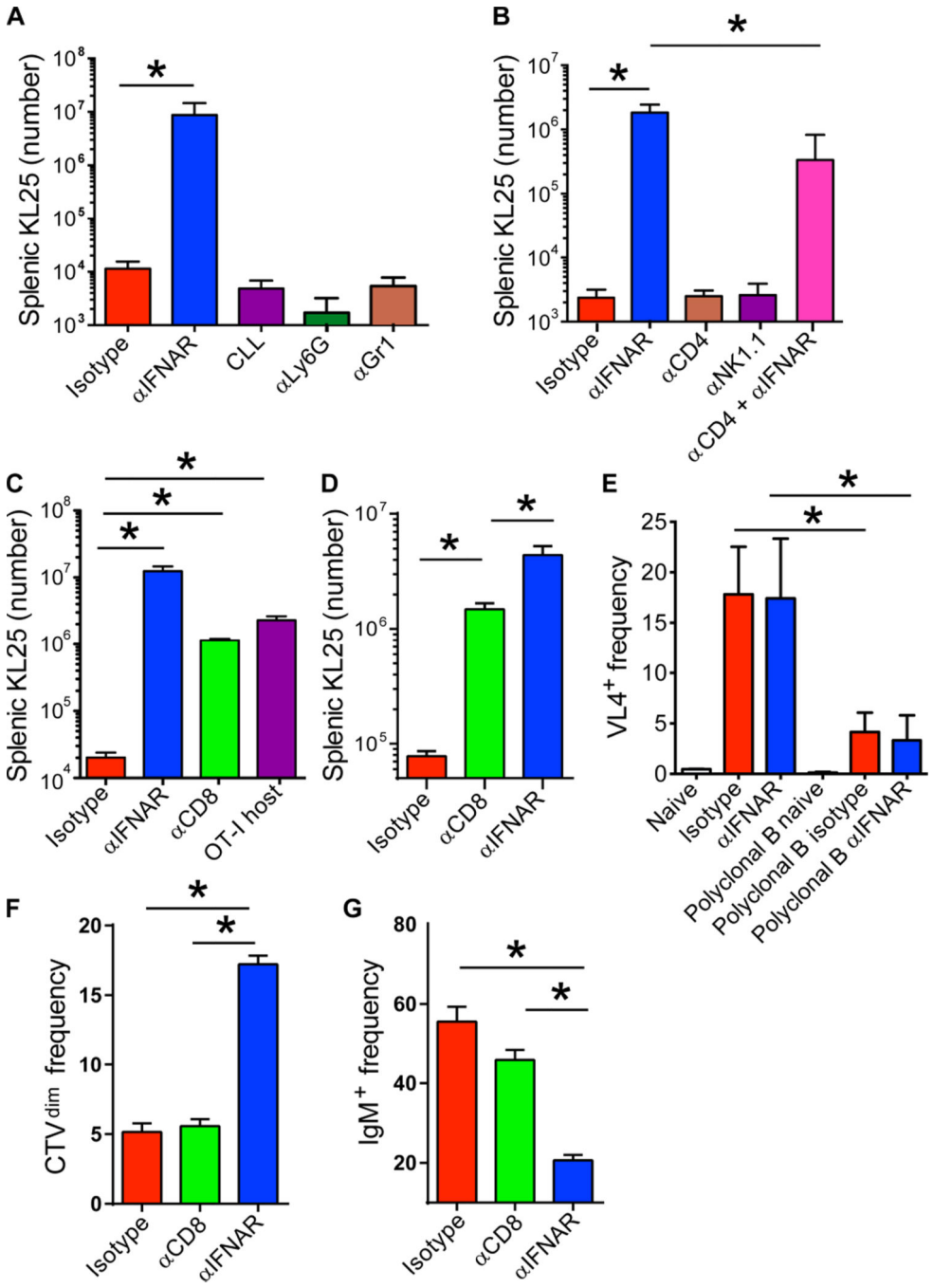

Fig. 4. LCMV-specific B cells are deleted by CD8$^+$ T cells

(**A**) Splenic KL25 counts from isotype, αIFNAR, CLL-depleted, Ly6G-depleted, and Gr1-depleted mice at 7 days after LCMV-M1 infection ($n = 4$ mice per group; two independent experiments; $*P < 0.05$). (**B**) Splenic KL25 counts from isotype, αIFNAR, CD4-depleted, NK cell–depleted, and CD4-depleted plus αIFNAR mice ($n = 3$ to 4 mice per group; two independent experiments; $*P < 0.05$). (**C**) Splenic KL25 counts from isotype, αIFNAR, CD8α-depleted, and OT-I TCR-tg mice at 7 days after infection ($n = 4$ to 5 mice per group; five independent experiments for CD8 depletion and two independent experiments for OT-I;

*$P < 0.05$). (**D**) KL25 H+L splenic counts from isotype, αIFNAR, and CD8α-depleted mice at 3 days after infection ($n = 3$ to 4 mice per group, representative of two independent experiments; *$P < 0.05$). (**E**) Frequency of LCMV (VL4) antigen–positive staining in KL25 or polyclonal WT B cells from naïve, isotype, or αIFNAR spleens at 26 hours after infection ($n = 4$ mice per group; two independent experiments; *$P < 0.05$). (**F** and **G**) Frequency of Cell Tracker Violet $(CTV)^{dim}$ KL25 (F) and IgM^{-} KL25 (G) among all splenic KL25 from isotype, αIFNAR, and CD8α-depleted mice at 3 days after infection ($n = 3$ to 4 mice per group; two independent experiments; *$P < 0.05$). For all plots, data are means + SD.

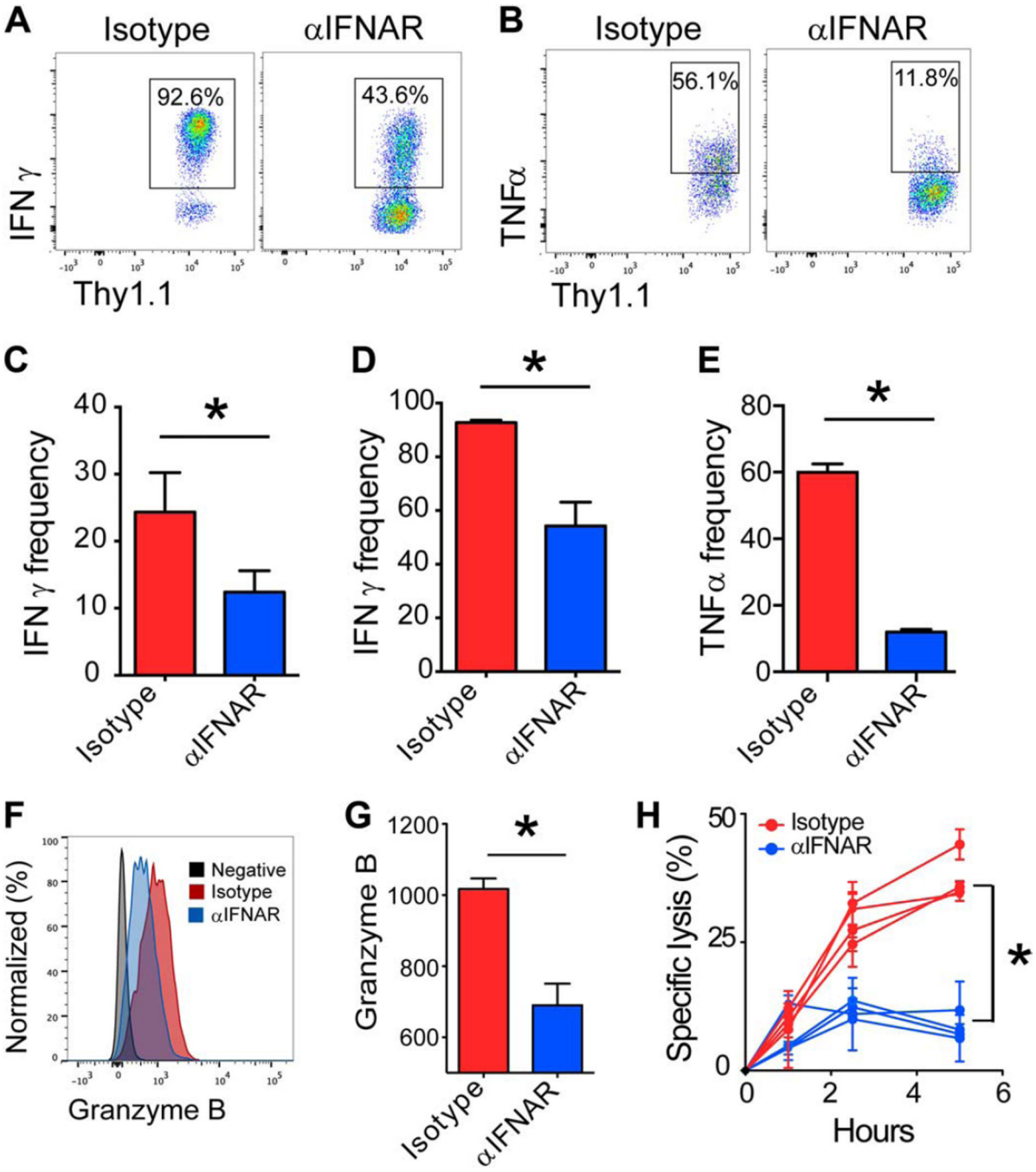

Fig. 5. Early CTL effector differentiation requires robust IFNAR signaling

(**A** and **B**) Representative FACS plots gated on Thy1.1$^+$ CD8α$^+$ P14 T cells showing the frequency (black boxes) of IFN-γ$^+$ (A) or TNFα$^+$ (B) production at 3 days after LCMV-M1 infection of isotype versus αIFNAR mice. (**C** to **E**) Quantification of IFN-γ or TNFα production by P14 cells from (A) and (B) in the presence (D and E) or absence (C) of cognate $GP_{33–41}$ peptide (n = 3 to 4 mice per group; three independent experiments; *P < 0.05). (**F**) Representative FACS histograms depicting granzyme B expression in Thy1.1$^+$ CD8α$^+$ P14 T cells in isotype (red) versus αIFNAR (blue) on day 4. Isotype control staining

is shown in gray. (**G**) Quantification of granzyme B geometric mean fluorescence intensity (GMFI) shown in (G) (n = 3 to 4 per group; two independent experiments; *P < 0.05). (**H**) Specific lysis of peptidepulsed targets by P14 T cells obtained from isotype-treated versus αIFNAR-treated mice at 3.5 days after LCMV-M1 infection (n = 4 mice per group; two independent experiments; *P < 0.05). For all plots, data are means + SD.

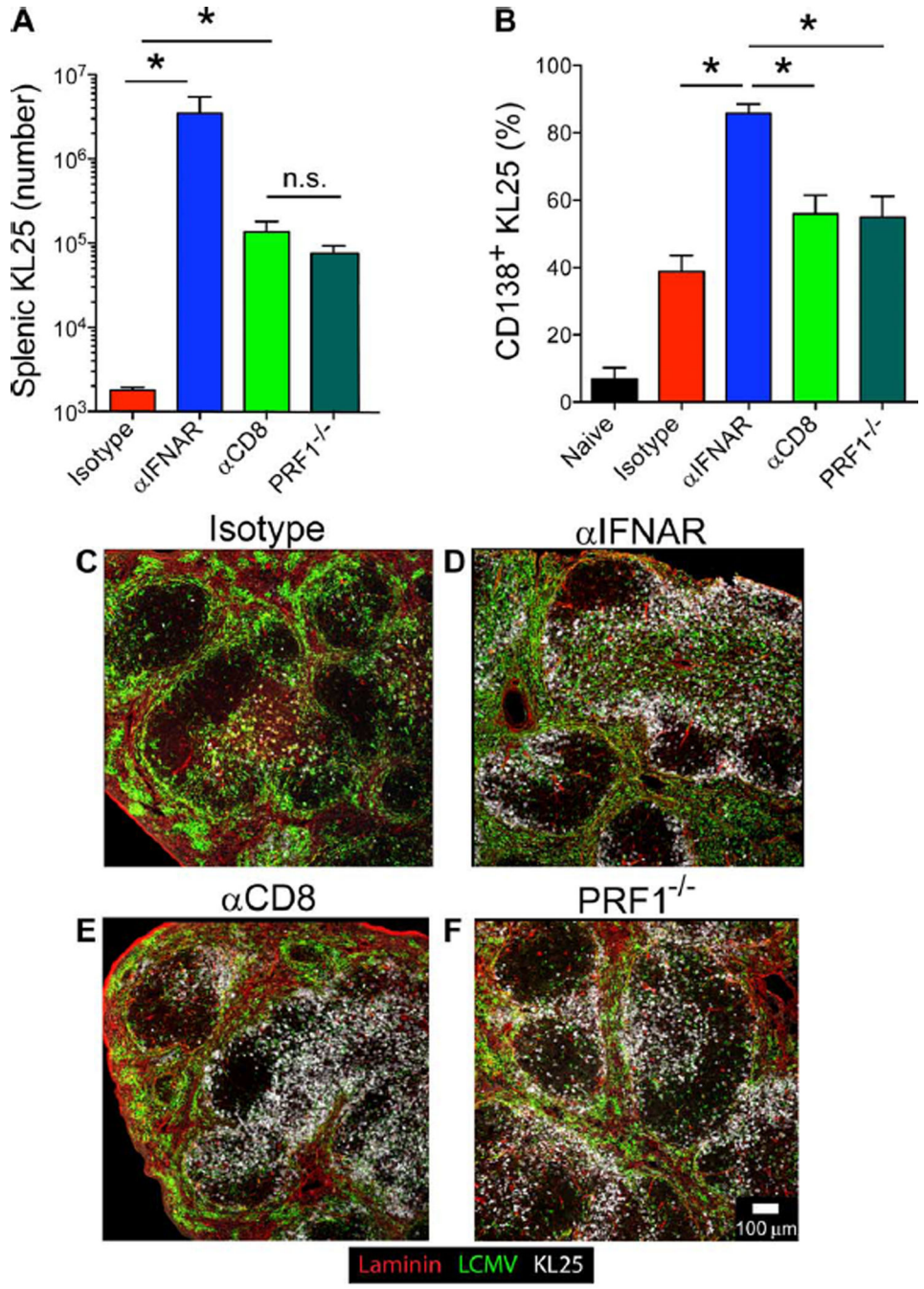

Fig. 6. Early IFNAR-dependent CTL removal of LCMV-GP B cells requires perforin

(**A**) Splenic KL25 counts from isotype, αIFNAR, CD8α-depleted, and PRF1-deficient animals at 7 days after LCMV-M1 infection (n = 3 to 4 mice per group; three independent experiments; *P < 0.05). n.s., not significant. (**B**) Frequency of CD138$^+$ ASCs among splenic KL25 B cells in naïve, isotype, αIFNAR, CD8α-depleted, and PRF1-deficient animals (n = 3 to 4 mice per group; three independent experiments; *P < 0.05). (**C** to **F**) Representative confocal images showing the anatomical distribution of CD45.1$^+$ KL25 H+L B cells (white) in the spleens of isotype (C), αIFNAR (D), CD8αdepleted (E), and PRF1-

deficient (F) recipients at 3 days after infection. Sections are also stained for laminin (red) and LCMV (green) (n = 3 mice per group; two independent experiments). For all plots, data are means + SD.

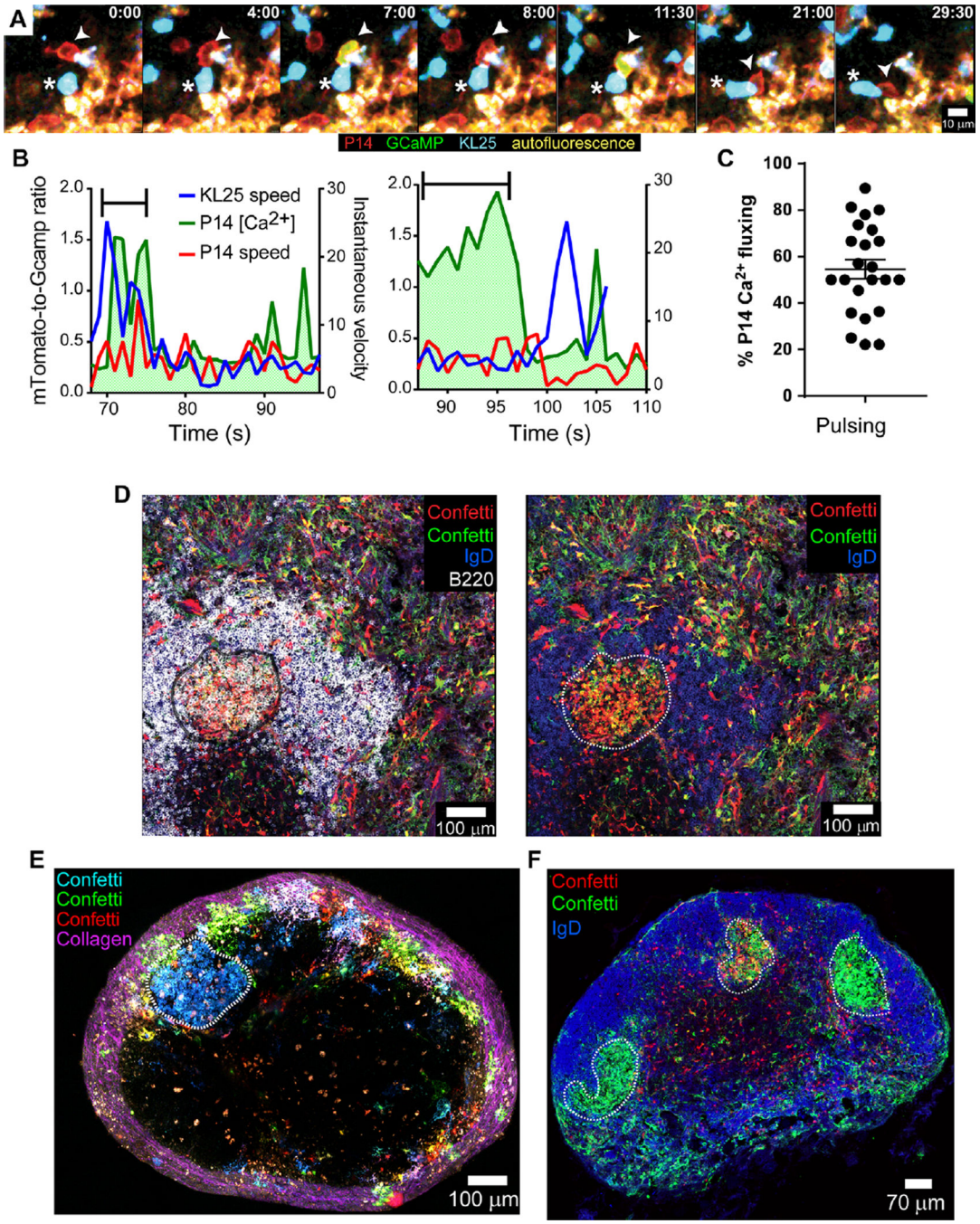

Fig. 7. CD8$^+$ T cells productively engage LCMV-infected KL25 B cells in vivo

(**A**) Representative 30-min time lapse in the day 3 LCMV-M1–infected spleen (captured by TPM) showing an mTomato$^+$ (red) GCaMP6s$^+$ (green) P14 CTL (arrow-head) engaging an mCerulean$^+$ KL25 B cell (blue cell with a white asterisk). See corresponding movie S4. (**B**) Representative plots depicting KL25 (blue) and P14 (red) instantaneous velocities, as well as P14 intracellular calcium concentration (green), for two distinct cell-cell interactions shown in movie S3. The period of direct interaction is highlighted with a black bracket. Note the elevation in intracellular P14 calcium during the bracketed interaction period. (A) and (B)

represent $n = 2$ to 3 mice per group (three independent experiments). (**C**) Percentage of P14 cells that flux calcium after interaction with KL25 H+L B cells ($n = 237$ interactions analyzed in twenty-four 5-min time intervals; $n = 4$ mice). (**D**) Representative confocal image captured in the spleen depicting clonal expansion of LCMV-infected GC B cells (white dotted line) in an αIFNAR-treated Confetti mouse at 39 days after r3LCMV-iCre infection. Other colors include B220 (white), IgD (blue), Confetti-cyan fluorescent protein (CFP; green), yellow fluorescent protein (YFP; green), green fluorescent protein (GFP; green), and Confetti-DsRed (red) ($n = 4$ mice per group; two independent experiments). (**E**) Representative mosaic captured by TPM of the entire popliteal lymph node showing an LCMV-infected clonal GC (blue cells; highlighted by a white dotted line) among the full range of fluorescent protein colors in a day 39 CD8-depleted r3LCMV-iCre–infected Confetti mouse. Second harmonic signal (collagen) is shown in purple ($n = 3$ mice per group; two independent experiments). (**F**) Representative confocal micrograph of a day 39 r3LCMV-iCre–infected popliteal lymph node from an αIFNAR-treated Confetti mouse revealing three distinct r3LCMV-iCre–infected clonal GCs (green; highlighted by white dotted lines), each with a different dominant clone (membrane-targeted Cerulean$^+$, cytosolic RFP$^+$, and nuclear-localized GFP$^+$; all visualized with anti-GFP) ($n = 4$ mice per group; two independent experiments). See corresponding movie S6.